Fast Registration Methodology for Fastener Assembly of Large-Scale Structure

Jing Xu, *Member, IEEE*, Rui Chen, Heping Chen, *Senior Member, IEEE*, Song Zhang, and Ken Chen

***Abstract*—Fastener assembly is a tedious and time-consuming work because operators have to check assembly manuals and find right fastener for each hole. Hence, this paper aims to develop a three-dimensional (3-D) projection system that projects assembly instruction onto the work piece surface directly to guide operators to assemble. However, in order to project the instruction accurately, the corresponding part of the computer-aided design model of the physical scanned area needs to be attained through the rapid and accurate registration. In order to achieve this goal, first, a high-accuracy and rapid 3-D measurement system is developed; second, a fast registration method based on local multiscale geometric feature vector is proposed to accelerate the registration speed and improve the registration reliability. Experimental results demonstrate the measurement accuracy of the developed system, and verify the feasibility of the proposed registration method. Hence, the proposed method can lead to improved assembly efficiency and decreased error probability, making great contributions to large-scale structure assembly.**

***Index Terms*—Augmented reality (AR), feature extraction, iterative closest point algorithm, pattern matching.**

I. Introduction

In the manufacturing of large-scale structure including commercial jets, trains, vessels, and space shuttles, the labor cost for fastener assembly takes up a large proportion of the total cost since there are thousands of kinds of fasteners to be inserted into hundreds of thousands of holes to connect the frame and the skin [1]. Thus, it takes a lot of time and labor to accomplish the assembly job.

Nowadays, the fastener assembly mainly depends on manual check of the design drawings and assembly instructions. The operators are demanded to look up in the assembly manuals to find correct radius and length of fastener for each hole in the computer-aided design (CAD) model of the large-scale structure and pick up the matching physical fastener and install it to correct physical hole. Thus, the process is tedious and time consuming. More significantly, errors are likely to occur during the prolonged manual check for operators, and irretrievable damage to the work piece would be done when the wrong fastener is assembled to the hole, leading to quality decrease and potential economic loss.

To assist mechanics and improve work efficiency, augmented reality (AR) has been applied in industrial manufacturing and maintenance. AR could overlay the artificial information directly on the physical, real-world object, which enables the operator to understand the knowledge about the object more intuitively and find the connection between the virtual data and the physical object. Thus, the application of AR in industrial manufacturing will improve the efficiency dramatically and make the procedure more user-friendly [2]–[7], e.g., in the assembly of an aircraft, a tablet personal computer (PC) equipped with a camera is used to capture the photo of the physical work piece, and assembly instruction will be shown above the photo on the screen [8]. However, operators have to hold the PC during the procedure, and switch observation between the screen and the actual workpiece repeatedly, leading to unnecessary work load.

Compared with hand-held display AR, spatial augmented reality (SAR) has the advantage that it augments real-world objects without the use of special displays such as monitors or handheld devices. SAR employs digital projectors to directly project virtual information onto physical objects [9]. The key advantage in SAR is that the projection is separated from the users of the system, which enables the operators to work more freely. Thus, SAR has become an emerging solution in industrial application [10]–[12], e.g., a SAR piping assembly facilitation system has been developed to guide assembly. It can provide operators with a direct view of instruction leading to improved accuracy and reduced cognitive workload [13]. Similarly, a SAR spot welding inspection system has been developed to facilitate inspection of the quality of spot welding [14]. In the proposed work, the three-dimensional (3-D) position of the physical object has to be known or additional markers are needed to register the physical object with the virtual CAD model.

The SAR system can project the necessary information including the fastener model and assembly instruction onto the proper location of the physical structure. However, for the large-scale structure, the biggest challenge is to locate the small scanned area in the entire CAD model because the limited field of view (FOV) of the projector can only cover a small part of the whole structure. In order to solve this problem, a creative fast registration method without additional markers is proposed to register the partial scanned area and the whole large-scale structure in this paper. For this purpose, the proposed method is supposed to have at least two capabilities.

Manuscript received December 17, 2015; revised April 18, 2016 and June 7, 2016; accepted June 30, 2016. Date of publication August 10, 2016; date of current version December 9, 2016. This work was supported in part by the National Natural Science Foundation of China under Grant 51105218 and in part by the State Key Laboratory of China under Grant SKLT2015B10. *(Corresponding author: Jing Xu.)*

J. Xu, R. Chen, and K. Chen are with the State Key Laboratory of Tribology, Department of Mechanical Engineering, Beijing Key Laboratory of Precision/Ultra-Precision Manufacturing Equipment Control, Tsinghua University, Beijing 100084, China (e-mail: jingxu@tsinghua.edu.cn; callmeray@163.com; kenchen@tsinghua.edu.cn).

H. Chen is with the Ingram School of Engineering, Texas State University, San Marcos, TX 78666 USA (e-mail: heping.chen@txstate.edu).

S. Zhang is with the School of Mechanical Engineering, Purdue University, West Lafayette, IN 47907 USA (e-mail: szhang15@purdue.edu).

Color versions of one or more of the figures in this paper are available online at http://ieeexplore.ieee.org.

Digital Object Identifier 10.1109/TIE.2016.2599140

First, the accurate and rapid 3-D shape measurement of scanned area of physical part is the prerequisite; otherwise, the incorrect 3-D shape measurement would lead to misalignment of scanned area of physical part and nonrapid measurement would result in inefficiency. So, a fringe-pattern-based real-time accurate 3-D measurement system is developed. To improve the measurement accuracy, the subpixel calibration method is also proposed.

Second, the automated and rapid registration algorithm is the key step. However, the traditional iterative closest point (ICP) registration method would take a long time for a large-scale registration without a proper initial guess; furthermore, an improper initial guess of the transmission matrix would lead to a local minima and failure for ICP registration. Thus, it is difficult for ICP to be directly used for the registration between a partial area and the whole large-scale object.

Recently, some registration methods based on geometrical feature have been proposed, such as D-4PCS [15], PFH [16], NDT [17], and NARF [18]. A point cloud registration method based on fast point feature histograms (FPFH) is proposed in 2009 [19], e.g., the FPFH is computed using certain relations between nearest neighbors and represents the model's property. But a large number of feature points are generated using this method, and random sampling is used during the alignment, which needs iterative computation, leading to huge computation amount and low efficiency. Another method based on scale invariant feature transform is proposed in 2010, where the SIFT algorithm is applied to attain point correspondence [20]. However, the SIFT algorithm cannot be used for smooth surface without a key feature point.

In order to accomplish the registration quickly and accurately, a new registration method based on local geometric feature combined with ICP registration is proposed, where local geometric feature is used to obtain the optimal initial guess for coarse registration and ICP is used for fine registration. Thus, the proposed registration method has high registration speed, accuracy, and reliability.

It is noted that above two capacities are also the two contributions of this paper.

The proposed system is capable of measuring the 3-D shape of the scanned area rapidly and locating this scanned area in the entire CAD model automatically and quickly, and then projecting the fastener model and assembly instruction onto the proper location of the assembled part. With the assistance of the proposed system, operators can pick right fastener for each hole to accomplish assembly task more rapidly and more accurately. More significantly, the developed system can be used in multitype structure manufacturing without any manual operation, thus making a big contribution to intelligent manufacturing.

The structure of this paper is as follows. In Section II, the work principle of the projection system is introduced. In Section III, the algorithm for high-accuracy rapid 3-D measurement is presented. In Section IV, the details of the proposed fast registration methodology based on local geometric feature are described. In Section V, some experimental application results are shown to demonstrate the feasibility of our system. Finally, In Section VI, our work and its impact are concluded briefly.

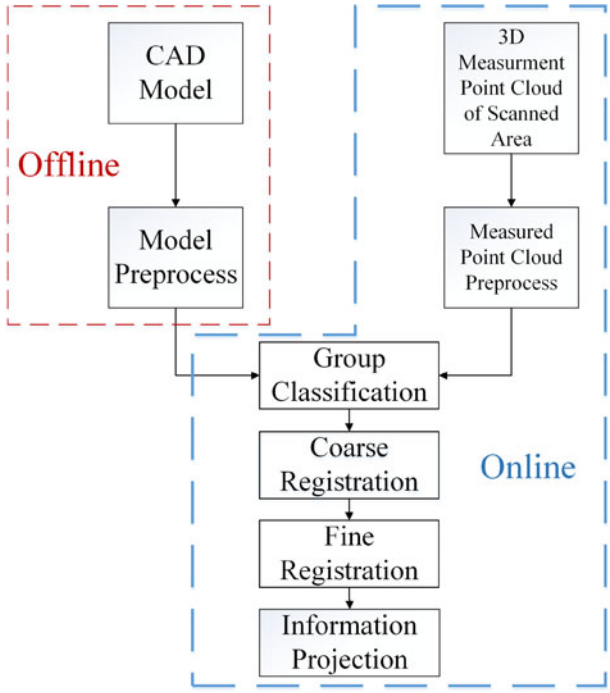

Fig. 1. Work principle.

II. Work Principle

The goal of the SAR fastener assembly projection system is to project the right fastener model information onto the proper location of the scanned area. To achieve this goal, we need to locate the scanned area in the whole CAD model, which needs the following process as shown in Fig. 1.

1) Accurate measurement, a 3-D measurement system is developed to measure the 3-D shape of the scanned area.
2) CAD model preprocess, in order to accelerate the registration, the local multiscale geometric feature vector (LMGFV) of every point in the CAD model is calculated.

   The first two processes are performed offline, which are needed to be performed only once for a specific CAD model, and the following processes are performed online.
3) The 3-D measurement point cloud of the scanned area is attained by measuring it with the system.
4) Measured point cloud process, the LMGFV for the center of the measurement point cloud is calculated.
5) Group classification, all the points of the CAD model are classified into different groups using a support vector machine (SVM).
6) Coarse registration, the belonging group and the closest point in the CAD model is identified, according to the LMGFV of the measurement point cloud, and the coarse location and range (the optimal initial guess for following ICP) in the CAD model for the measurement point cloud is attained.
7) Fine registration, according to the result of coarse registration, the measurement point cloud is registered with the chosen area of the CAD model using ICP.

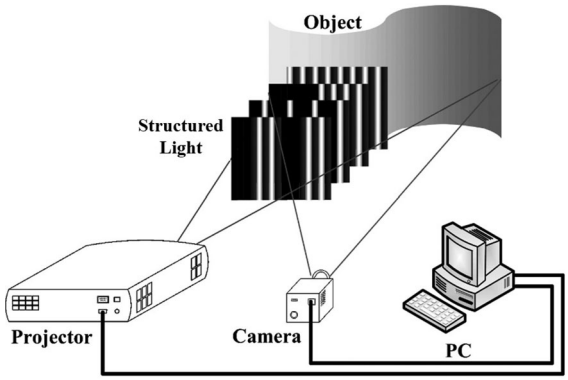

Fig. 2. Three-dimensional measurement setup.

8) Information projection.
After the fine registration, the positions of holes related to the projector, where information needs to be projected, are attained. Then, the fastener model and the assembly instruction can be projected to the proper location of the physical work piece.

III. Three-Dimensional Measurement

The accurate 3-D shape of the scanned area has to be measured rapidly before registration. So a high-accuracy 3-D measurement system based on structured light is developed. First, the projector shoots structured light such as fringe patterns to the work piece to assemble, and then deformed structured light is captured by the camera and decoded by PC. After the decoding, the 3-D shape is attained by triangulation. Fig. 2 shows the 3-D measurement setup.

According to the principle described above, the calibration accuracy for the measurement system determines the measurement accuracy and further the registration accuracy. Thus, a high-accuracy calibration algorithm is desired and proposed. In this paper, a plane-based calibration algorithm is applied [21].

Assuming that the coordinate of the calibration board in the world coordinate system (WCS) is $Z_W = 0$. Then, the camera projection equation can be simplified to

$$\lambda \begin{bmatrix} u_C \\ v_C \\ 1 \end{bmatrix} = K_{\text{int}}[r_1, r_2, r_3, t] \begin{bmatrix} X_W \\ Y_W \\ 0 \\ 1 \end{bmatrix} = K_{\text{int}}[r_1, r_2, t] \begin{bmatrix} X_W \\ Y_W \\ 1 \end{bmatrix} \quad (1)$$

where λ is the scale coefficient, u_C and v_C are the 2-D image pixel coordinates, K_{int} is the intrinsic parameter matrix for the camera or projector, r_1, r_2, r_3, and t are the rotation and translation vectors of the extrinsic parameter matrix, and X_W, Y_W, and Z_W are the 3-D world coordinates.

While X_W and Y_W represent the world coordinates of the markers on the calibration board, which are given and accurate, the acquisition accuracy of the 2-D image pixel coordinates determines the calibration accuracy. Hence, a subpixel edge detection algorithm is proposed for improved calibration precision.

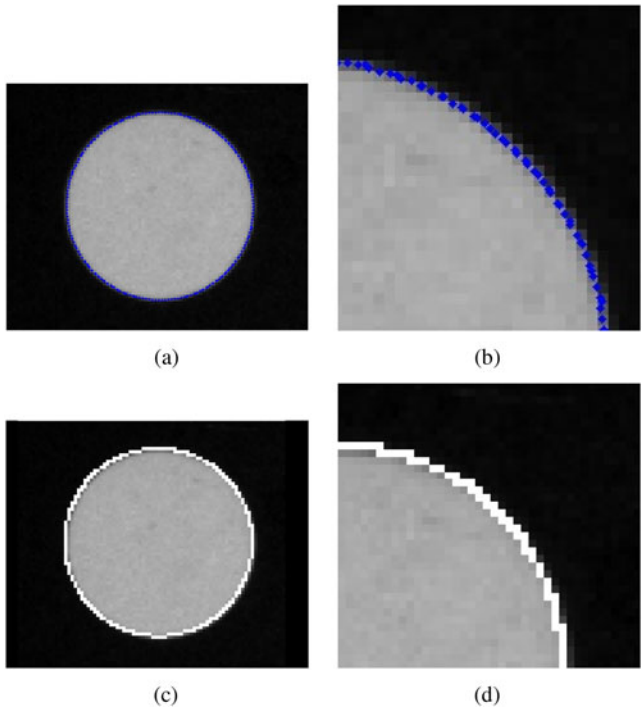

Fig. 3. Edge detection results: (a) Subpixel edge detection result; (b) partial enlarged view of (a); (c) Canny edge detection result; and (d) partial enlarged view of (c).

Compared with the pixel-level accuracy of the Canny edge detection [22], the accuracy of the proposed edge detection algorithm is improved to the subpixel level, as shown in Fig. 3, thus improving the calibration accuracy greatly.

In this paper, sinusoidal fringe phase shift and a dual-frequency phase unwrapping method are used to attain the projector absolute phases rapidly[23]–[26]. Then, the 3-D coordinates of the points can be computed by triangulation using the absolute phases and the camera image pixel coordinates.

IV. Registration Method

Once the measurement of the scanned area is done, automatic registration between it and the large-scale CAD model is needed to locate the scanned area at the structure. However, for large-scale part registration, the traditional ICP registration method would take a long time, even fail without a proper initial guess of position and orientation. Thus, in this paper, a fast registration methodology based on LMGFV is proposed as the initial guess for ICP, which provides a coarse range and an initial transformation matrix. In this method, a coarse registration using LMGFV is first deployed to attain the approximate position, orientation, and range of the partial area to be registered in the entire object, then the fine registration is applied to attain the accurate translation relationship between the scanned area and the specified region of the large-scale structure using ICP algorithm. Thus,

the proposed registration method has high registration speed, accuracy, and reliability.

A. LMGFV Generation

Due to its invariability to translation and rotation, curvature of surface point is deployed as the persistent feature in a rapid coarse registration. Polynomial fitting is applied to calculate the curvature of local surface because of its simple computational algorithm and high robustness [27]–[29]. However, if only the curvature of the point is used to register, some ambiguity still exists, because many surface points of the large-scale structure may have similar curvature. Hence, the LMGFV is proposed to eliminate the ambiguity.

For one candidate surface point p_M in the CAD model, several spheres are set up with p_M as their centers and their radii range from r to Nr, where r and N, respectively, represent the sample resolution and range of LMGFV. It is noted that the biggest sphere with radius of Nr should be comparable to the maximum range of the scanned area.

For one specific sphere S_i with a radius of ir $(i = 1, 2, \ldots, N)$, the weighted mean value f_i and weighted second moment d_i of the curvatures of all the points within S_i are calculated and taken as the curvature distribution feature parameters of S_i

$$\begin{aligned} f_i &= \frac{1}{n_i}\sum W_j \tau_j \\ d_i &= \frac{1}{n_i}\sqrt{\sum W_j {\tau_j}^2} \end{aligned} \tag{2}$$

where W_j is the weighing factor. Because of the measurement point cloud, the point cloud density may be different at different parts. In order to eliminate the effect of the density variety, the weighing factor W_j is set inversely proportional to the point cloud density. Furthermore, the LMGFV X_M is obtained by combining the curvature distribution feature parameters of all the spheres $F = \{f_i\}$, $D = \{d_i\}$. Thus, the LMGFV X_M represents the curvature distribution feature of the neighboring surface of point p_M, which will be used in point group classification and further registration.

B. Group Classification Using SVM

Due to its solid theoretical foundation, SVM, a supervised machine learning model, is used widely for group classification and regression analysis [30]–[33]. In this paper, SVM is used to perform group classification of the CAD model in order to speed up the following registration.

For a set of input data $\{(X_1, y_1), (X_2, y_2), \ldots, (X_n, y_n)\}$, where each X_i represents the LMGFV of one point in the CAD model and y_i represents the corresponding belonged group label of the point, SVM is applied to obtain the classification function $f(X)$, which divides all the points into its belonged group

$$f(X) = \omega^T X + \delta. \tag{3}$$

For the CAD model, the LMGFV of each point in the CAD model is calculated, and the points of different parts, such as wings and tails, are labeled with different numbers. Then, a number of points of each part are chosen to train the SVM to attain the classification function.

Once the classification function $f(X)$ is attained, it will be applied to obtain the belonged group of the measurement point cloud.

C. LMGFV Distance

In order to calculate the similarity of the LMGFVs of two points, the LMGFV distance is proposed.

For two candidate points E and J, the LMGFVs of the two points are X_E and X_J, the length of which is $2M$

$$\begin{aligned} X_E &= \{F_E, D_E\} \\ &= \{f_{E1}, f_{E2}, \ldots, f_{\mathrm{EM}}, d_{E1}, d_{E2}, \ldots, d_{\mathrm{EM}}\} \\ X_J &= \{F_J, D_J\} \\ &= \{f_{J1}, f_{J2}, \ldots, f_{\mathrm{JM}}, d_{J1}, d_{J2}, \ldots, d_{\mathrm{JM}}\}. \end{aligned}$$

The LMGFV distance between E and J $Q(E, J)$ is the following:

$$\begin{aligned} Q(E, J) = W_F \sqrt{\sum_{i=1}^{M} W_{fi}(f_{Ei} - f_{Ji})^2} \\ + W_D \sqrt{\sum_{i=1}^{M} W_{di}(d_{Ei} - d_{Ji})^2} \end{aligned} \tag{4}$$

where W_F and W_D represent the weighing factor of the mean value vector difference and the second moment value vector difference, respectively, and W_{fi} and W_{di} represent the weighing factor of each element in the vector.

Because f_i and d_i represent the distribution feature of the curvature of all the points within the sphere with radius of ir, when $i = 1$, the sphere is the smallest one, containing the fewest points, and f_1 and d_1 represent the distribution feature of the curvature at the center of the sphere more accurately than f_i and d_i. Hence, the W_{fi} and W_{di} are set smaller when i becomes bigger.

After the distance of the two LMGFV $Q(E, J)$ is calculated, the similarity of E and J is attained. When the distance is small, it means the neighborhoods of these two points have similar curvature distribution.

D. Connected Point Cloud Within Sphere

For the LMGFV generation for the CAD model point cloud, if all the points within one sphere are involved to the calculation, it would lead to calculation error because there are two kinds of points that are not included in the measurement point cloud and should be excluded. The first kind of points are those that are not connected to the center point, and the second kind are those that are connected but blocked and cannot be measured by the system.

Above points are not included in the sphere with same radius in the measurement point cloud, thus they should be excluded for the LMGFV generation for the CAD model. As shown in

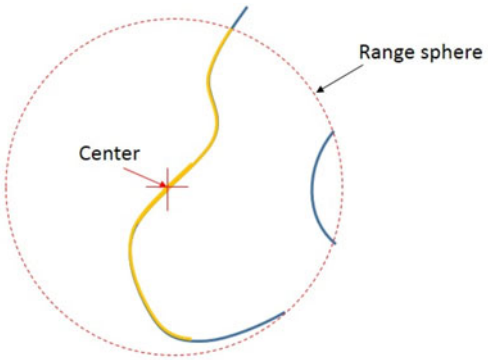

Fig. 4. Entire point cloud and connected point cloud within a sphere.

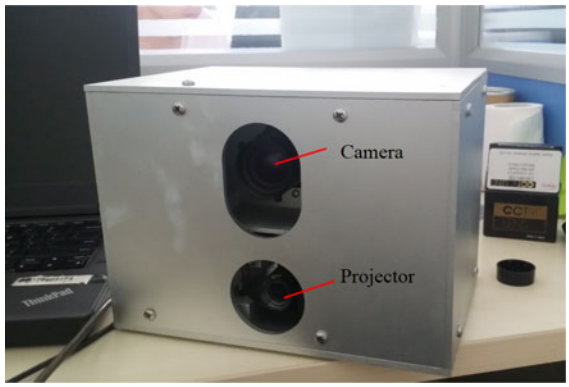

Fig. 5. Projection and measurement system setup.

Fig. 4, blue points represent the CAD model, and yellow points represent the desired connected point cloud.

The connected point cloud within the sphere is obtained to generate the LMGFV as follows.

1) The connectivity data of the points are obtained when the CAD model is converted to the point cloud.
2) The normal vector of all the points are calculated using plane fitting.
3) For one candidate point as the center of the sphere, the connected point cloud grows from it: points that are connected to the center point are first included, then points connected to the existing point cloud are added to the connected point cloud until the 3-D distance to the center point is larger than the radius or the normal vector of it is reversed to the center point.

After the connected point cloud is obtained, the LMGFV for the center point is created using the curvature of all the points contained in it for group classification and further registration.

E. Measured Point Cloud Range and Center

For the measurement point cloud which is obtained by the 3-D measurement system, it may not have the same range in all directions. But for the point cloud of the CAD model, it would have same range in all directions. Thus, if a sphere with improper radius is used to calculate the LMGFV of the measurement point cloud, it would include more points in some directions than others, which would lead to the calculation error. In order to solve this problem, the center and range of the measurement point cloud are attained using following method.

The 3-D coordinates of the measurement point cloud are in the camera coordinate system. Because the optical axis of the camera is set almost vertical to the measured surface, the measurement point cloud is in the xy plane approximately. Thus, the point whose x and y coordinates are closet to the x and y coordinates gravity center is set as the center of the measurement point cloud. If the maximum distance of the measurement point cloud from the center in eight directions is obtained, then the range of it is set to the minimum value of the eight distances, in order to guarantee that for one sphere in range, it would have same distance in all the directions in the measurement point cloud. Thus, the LMGFV of the measurement point cloud can be comparable to the LMGFV of the CAD model.

F. Registration Process

The rapid registration process based on LMGFV is described as follows.

First, the offline preprocess for the whole CAD model of the large-scale structure are performed as follows.

1) The CAD model is converted to point cloud set $\{p\}$ and downsampled to reduce unnecessary computational complexity.
2) Gaussian curvature τ of every point of $\{p\}$ is calculated using the algorithm as described above.
3) The LMGFV X of every point is obtained as described above.

Then, we operate the measurement point cloud as follows.

1) Gaussian curvature τ for all the points of the measurement point cloud is calculated.
2) The center of the point cloud G_{MS} and the point cloud range M are attained.
3) The LMGFV for the measurement point cloud X_{MS} with length of $2M$ is generated.

Then, the online coarse registration is performed as follows.

1) The LMGFV for the CAD model is set to the same length of X_{MS}, and the SVM group classification is done.
2) The belonged group of X_{MS} is attained, and the point in the CAD model G_{CAD} with the most similar LMGFV is searched in the specific group.

After the approximate location and range of the measurement point cloud in the whole CAD model are attained, the final fine registration is applied to obtain the accurate translation matrix using ICP.

V. Experiments and Discussions

A high-accuracy projection and measurement system composed of a camera and a projector is set up as shown in Fig. 5.

The camera is a monochrome JAI SP-5000M-USB camera with a pixel depth of 8 bits, a resolution of 2560 $\times$ 2048, and a frame rate of 120 f/s. The projector is a DLP Lightcrafter

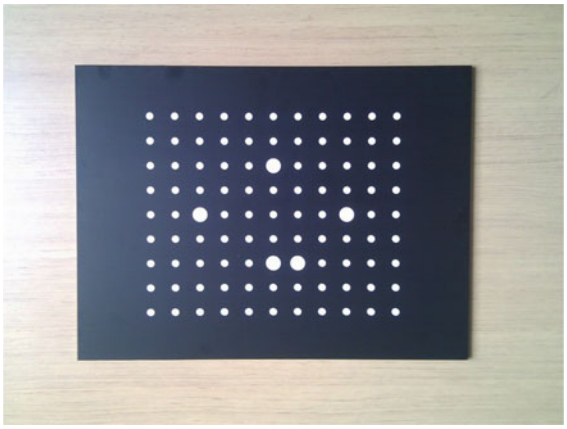

Fig. 6. Calibration board.

4500 manufactured by TI with a resolution of 912×1140. The maximum projection frame rate of the projector is 4225 f/s for 1-bit images and 120 f/s for 8-bits images. The position relationship between the camera and the projector is kept unchanged by fixing both of them within a box.

First, in order to verify the measurement accuracy of our system, a calibration board is measured as shown in Fig. 6.

Before the measurement, the system needs to be calibrated accurately, where the intrinsic parameter of the camera and the projector and also the relative position of them are attained. Table I shows the calibrated parameter of the system attained by our proposed method.

The reprojection error of the projector is 0.0815 pixels, and that of the camera is 0.1374 pixels. The conventional calibration reprojection error of the camera and projector is 0.1133 and 0.3274 pixels, respectively [34]. The comparison result demonstrates that the proposed method leads to an improvement of calibration accuracy.

Then, the 3-D coordinates of the reference dots are measured and transformed to the WCS. The accuracy of our system can be verified by comparing the measured 3-D world coordinates of the dot centers with the known positions. The measurement errors are shown in Fig. 7 and Table II. The result demonstrates the good accuracy of our system, with an RMS error of 0.0586 mm for 3-D measurement.

In the second experiment, an aircraft model as shown in Fig. 8 is measured to verify the proposed rapid registration method.

First, the CAD model is converted to point cloud and downsampled as shown in Fig. 9. The total number of points is 597 529, and the LMGFV of every point in it is calculated. For the measurement prototype, the maximum range of the scanned area is about 100 mm. Hence, the sample resolution r is set to 10 mm, and the range N is set to 10. Second, the 3-D shape of a local area of the model is measured by our system and a point cloud with 49 889 points is attained as shown in Fig. 10.

Before the proposed method is carried out, the traditional ICP registration method is performed. Fig. 11 is the registration result using the ICP method without initial guess, where the green points represent the CAD model and the red points represent the measurement point cloud, which illustrates that the traditional ICP method cannot be used directly in the registration between a partial area and the whole large-scale object. Then, the ICP registration is performed between the measurement point cloud and the right part of the whole model without initial guess of transformation matrix. Fig. 12 shows the registration result, where blue points represent the right part, and red points represent the measurement point cloud. As shown in the figure, ICP registration method turns out failure without a coarse initial guess of the transformation matrix. Aforementioned experiments illustrate that the right part of the whole model and a coarse initial guess of the transformation matrix are the perquisites for the correct ICP registration, which are what the proposed method provide.

The center point of the measurement point cloud G_{MS}, the point cloud range M and further the LMGFV of the center point X_{MS} are computed using the method described in Section IV. The radius of the sphere is 76.69 mm, thus M is set to 8. Then, the LMGFVs of the CAD model are set to the length of the LMGFV of center point and classified to four groups as shown in Fig. 13, where different color represents different group.

Then, the belonged group of X_{MS} is attained, and the point with the most similar LMGFV G_{CAD} is searched in the specific group. And the approximate location and range of the measurement point cloud in the whole CAD model are attained. Finally, the fine registration is applied to obtain the accurate translation matrix using ICP. The coarse registration and fine registration results are shown in Fig. 14, where the green points represent the CAD model, the blue points represent the coarse registration local region of the CAD model, and the red points represent the fine registration result.

The computational efficiency of the proposed method and the traditional ICP algorithm is compared. The time costs of the two methods are shown in Table III, where the ICP algorithm is 45 763 s, while our proposed method is only 27.134 s. The preprocess for the CAD model, downsampling and LMGFV generation, takes around 734 s. But the preprocess needs to be performed only once offline for one specific CAD model. The comparison result proves that the application of our proposed registration method leads to a drastically improved computation efficiency.

The requisite for correct registration is the accurate acquirement of the LMGFV of the scanned area, which describes the distribution of curvature. Because the curvature of the point is calculated using surface fitting and the other side of the edge points is missing, so if the outer side of the edge is smooth extension or nothing, the calculation error of the edge points curvature is small; otherwise, if the outer side of the edge has a widely different curvature, it will lead to calculation error of curvature and further wrong registration. Furthermore, because the registration algorithm is based on the distribution of curvatures, some ambiguities may occur when there are large areas of flat surface. But the distribution of fastener holes

TABLE I
CALIBRATION RESULT

	Intrinsic Parameter				Relative Position				
Camera	2545.470	0	1284.410		0.999	0.0003	-0.0091		1.655
	0	2545.614	1009.586						
	0	0	1	Rpc	-0.0025	0.999	0.0097	Tpc	-85.032
Projector	1149.008	0	4431.094						
	0	2300.890	1186.827		0.0091	-0.0097	0.999		-9.322
	0	0	1						

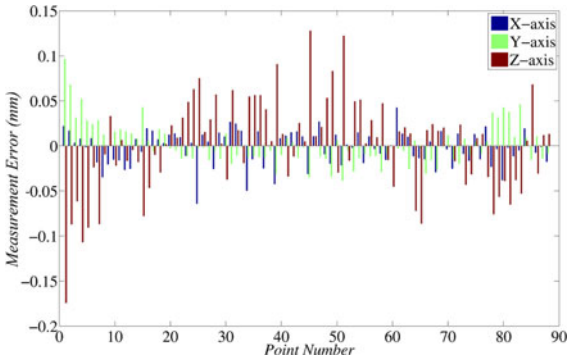

Fig. 7. Measurement errors.

TABLE II
MEASUREMENT ERROR

Directions	Maximum(mm)	RMS error(mm)
X-axis	0.0642	0.0190
Y-axis	0.0965	0.0228
Z-axis	0.1744	0.0505
3-D	0.2006	0.0586

Fig. 8. Aircraft model for the registration experiment.

would help eliminate some ambiguities, and if an error occurs, the operators would choose the correct projected information manually.

Once the registration is done, the relative position from the scanned area to the projection system is attained, as shown in Table IV. Then, the assembly information is projected onto the proper location of the work piece surface, as shown in Fig. 15,

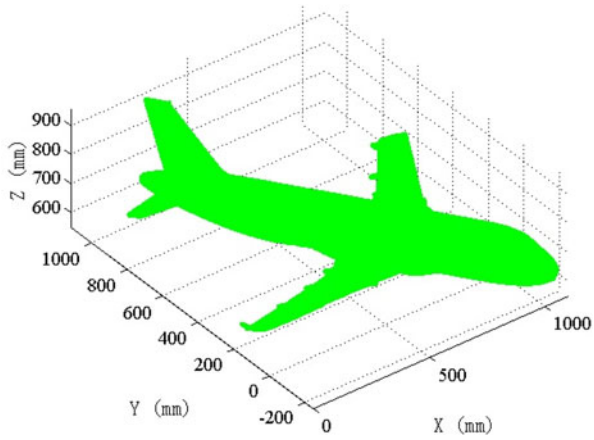

Fig. 9. CAD model point cloud.

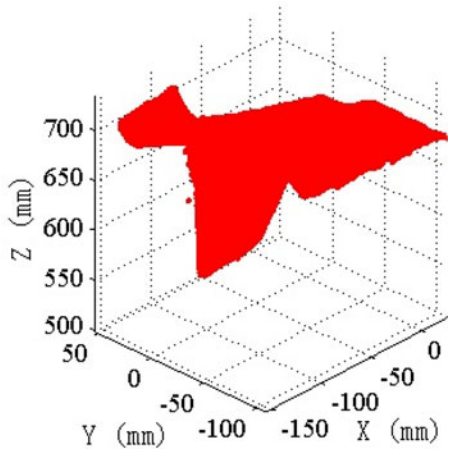

Fig. 10. Measured point cloud.

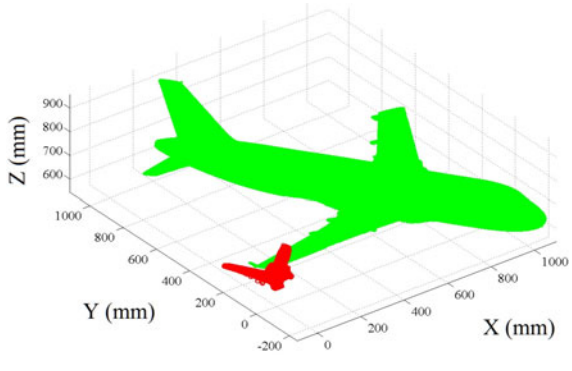

Fig. 11. Registration result using the ICP method directly.

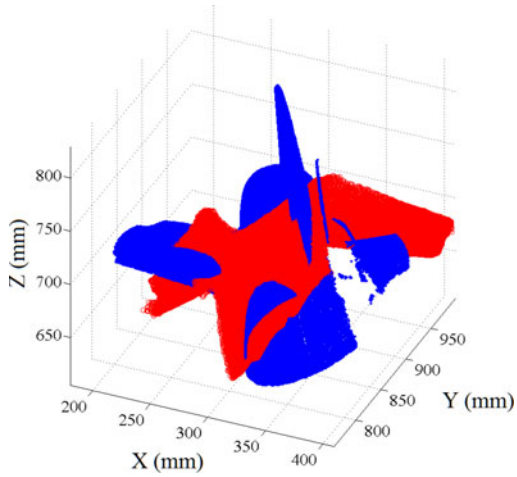

Fig. 12. Registration result using the ICP method between the measurement point cloud and the right part of the whole model without initial guess of transmission matrix.

TABLE III
TIME COST FOR ICP METHOD AND PROPOSED METHOD

Method	ICP algorithm	Proposed method
Online registration	45763 s	27.134 s

TABLE IV
RELATIVE POSITION FROM THE PROJECTED AREA TO THE PROJECTION SYSTEM

R			T(mm)
0.77495	− 0.59947	0.20023	842.1565
− 0.20126	0.06625	0.97729	386.4050
− 0.59912	− 0.79765	− 0.06930	− 195.887

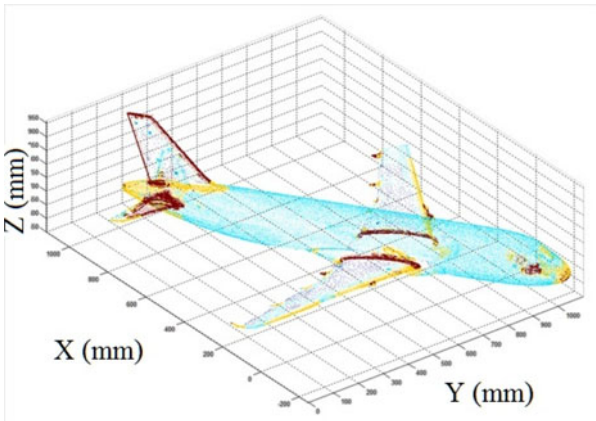

Fig. 13. Group classification result.

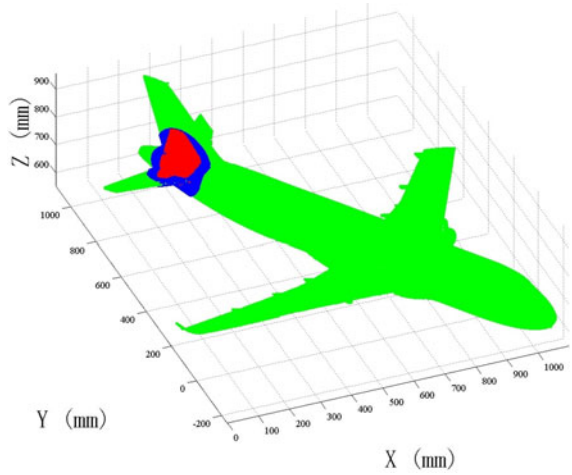

Fig. 14. Registration result.

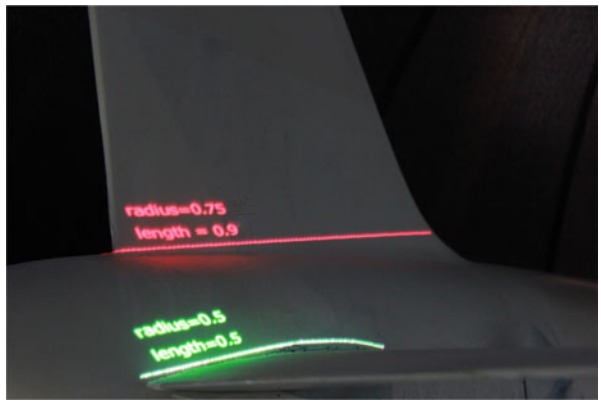

Fig. 15. Projected assembly information.

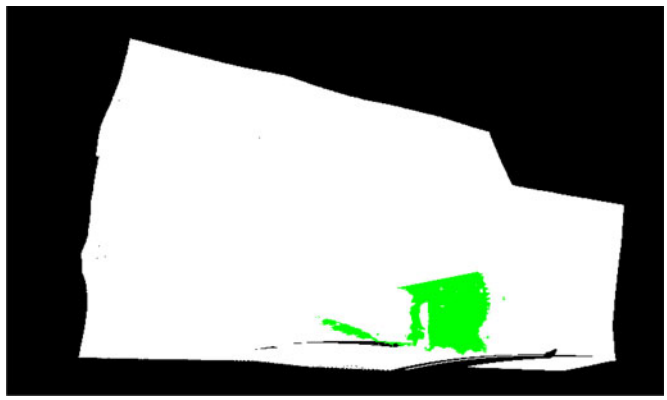

Fig. 16. Real-scale registration result.

where different colors represent information of different fastener models. With the assistance of our projection system, the process of checking manuals is eliminated, and operators are able to assemble with higher efficiency and fewer errors.

Then, a real-scale experiment is carried out, wherein an off-the-shelf ultrashort throw projector with resolution of 1920 × 1080 is used. A workpiece with a size of 5m × 3m is set up by using aluminum frames, aluminum plates, and white plastic plates. The workpiece is first measured by the laser radar, and the result is used as the CAD model. Then, a part of the workpiece is measured by the system and registered using the proposed method. The registration result is shown in Fig. 16. After the

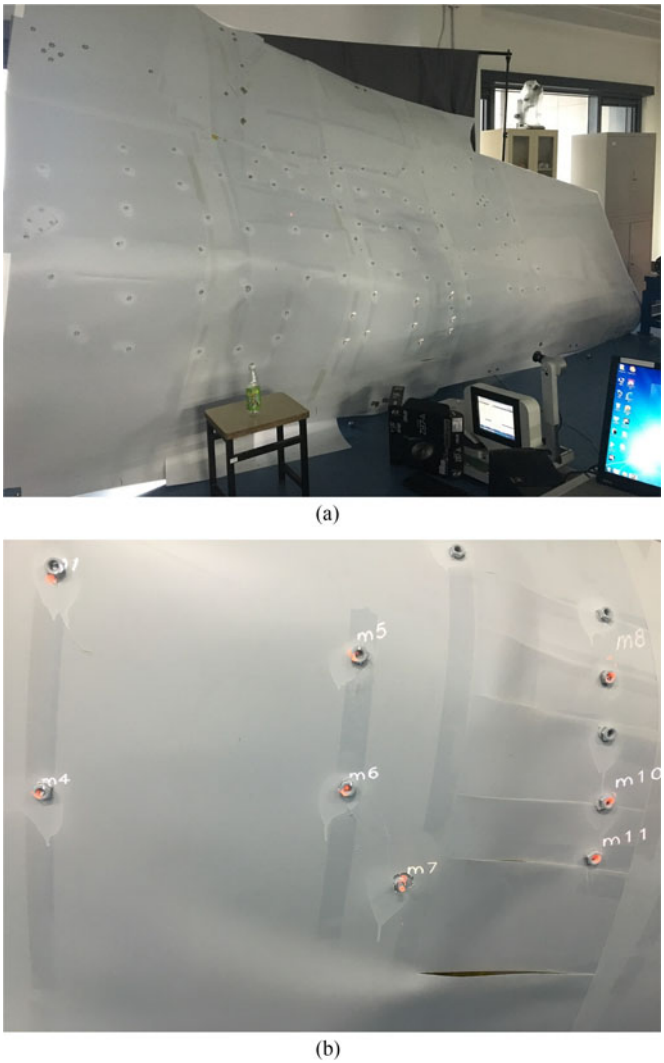

Fig. 17. Real-scale information projection.

registration, the fastener information in the FOV of the projector is projected onto the workpiece surface as shown in Fig. 17.

VI. Conclusion and Future Work

In the current fastener assembly for the large-scale structure, paper-based manual checking is still the main solution, which leads to low efficiency and high probability of error. Hence, in this paper, a novel high-accuracy projection system was developed, which will measure the 3-D shape of the workpiece, load assembly information, and project instructions onto the proper location of the structure surface. However, the registration between the scanned area and the whole CAD model needs to be performed accurately, which cannot be accomplished using the traditional ICP method. Thus, a new fast registration methodology based on LMGFV combined with ICP was proposed in this paper.

Accurate and fast measurement of the 3-D shape of the scanned area is the basis of registration. Hence, an accurate calibration method using subpixel edge detection and ellipse fitting was proposed in this paper to improve the measurement accuracy of the system. The proposed registration method was demonstrated to speed up the registration process than using ICP alone. The experimental results verify the effectiveness of our method and also validate the feasibility of the application of the system in industrial manufacturing.

With the help of the system, workers will see the assembly instruction directly and are able to assemble without manual check, thus improving the assembly efficiency drastically and lowering the probability of error. Furthermore, the developed system is applicable to mutlitype structure manufacturing, which makes a great contribution to intelligent manufacturing.

References

[1] Y. Jin, R. Curran, J. Butterfield, R. Burke, andB. Welch," Intelligent assembly time analysis, using a digital knowledge based approach," *J. Aerosp. Comput. Inf. Commun.*, vol. 6, no. 8, pp. 506–522, Aug. 2009.

[2] T. P. Caudell and D. Mizell, "Augmented reality: An application of heads-up display technology to manual manufacturing processes," in *Proc. Hawaii Int. Conf. Syst. Sci.*, Jan. 1992, pp. 659–669, doi: 10.1109/HICSS.1992.183317.

[3] R. Azuma, Y. Baillot, R. Behringer, S. Feiner, S. J. Julier, and B. Macintyre,"Recent advances in augmented reality," *IEEE Comput. Graph.*, vol. 21, no. 6, pp. 34–47, Nov./Dec. 2001.

[4] S. K. Ong, M. L. Yuan, andA. Y. C. Nee,"Augmented reality applications in manufacturing: A survey," *Int. J. Prod. Res.*, vol. 46, no. 10, pp. 2707–2742, Mar. 2008.

[5] A. Y. C. Nee, S. K. Ong, G. Chryssolouris, and D. Mourtzis, "Augmented reality applications in design and manufacturing," *CIRP Ann.-Manuf. Technol.*, vol. 61, pp. 657–679, Jun. 2012.

[6] A. D. Cheok, Y. Qiu, K. Xu, and K. G. Kumar,"Combined wireless hardware and real-time computer vision interface for tangible mixed reality," *IEEE Trans. Ind. Electron.*, vol. 54, no. 4, pp. 2174–2189, Aug. 2007.

[7] R. Marin, P. J. Sanz, P. Nebot, and R. Wirz,"A multimodal interface to control a robot arm via the web: A case study on remote programming," *IEEE Trans. Ind. Electron.*, vol. 52, no. 6, pp. 1506–1520, Dec. 2005.

[8] J. Servan, F. Mas, J. L. Menendez, and J. Rios, "Assembly work instruction deployment using augmented reality," in *Key Eng. Mater.*, Jul. 2012, pp. 25–30.

[9] C. Menk, E. Jundt, and R. Koch, "Visualisation techniques for using spatial augmented reality in the design process of a car," *Comput. Graph. Forum*, vol. 30, pp. 2354–2366, Oct. 2011.

[10] M. Zaeh and W. Vogl, "Interactive laser-projection for programming industrial robots," in *Proc. IEEE/ACM Int. Symp. Mixed .Augmented Reality*, Santa Barbara, CA, USA, Oct. 2006, pp. 125–128.

[11] A. Olwal, J. Gustafsson, and C. Lindfors, "Spatial augmented reality on industrial CNC-machines," *Proc. SPIE Electron. Imag.*, vol. 6804, Feb. 2008, Art. no. 680409.

[12] S. R. Porter, M. R. Marner, R. T. Smith, J. E. Zucco, and B. H. Thomas, "Validating spatial augmented reality for interactive rapid prototyping," in *Proc. 9th IEEE Int. Symp. Mixed Augmented Reality*, Seoul, South Korea, Oct. 2010, pp. 265–266.

[13] J. Zhou, I. Lee, B. Thomas, R. Menassa, A. Farrant, and A. Sansome, "In-situ support for automotive manufacturing using spatial augmented reality," *Int. J. Virtual Reality*, vol. 11, pp. 33–41, Nov. 2012.

[14] L. Hou, X. Wang, and M. Truijens, "Using augmented reality to facilitate piping assembly: An experiment-based evaluation," *J. Comput. Civil Eng.*, vol. 29, Jul. 2013, Art. no. 05014007.

[15] J. P. Da Silva, D. L. Borges, and F. de Barros Vidal, "A dynamic approach for approximate pairwise alignment based on 4-points congruence sets of 3D points," in *Proc. 18th IEEE Int. Conf. Image Process.*, Brussels, Belgium, Sep. 2011, pp. 889–892.

[16] R. B. Rusu, Z. C. Marton, N. Blodow, and M. Beetz, "Learning informative point classes for the acquisition of object model maps," in *Proc. 10th Int. Conf. Control, Autom., Robot. Vis.*, Hanoi, Vietnam, Dec. 2008, pp. 643–650.

[17] T. Stoyanov, M. Magnusson, H. Almqvist, and A. J. Lilienthal, "On the accuracy of the 3D normal distributions transform as a tool for spatial representation," in *Proc. IEEE Int. Conf. Robot. Autom.*, May 2011, pp. 4080–4085.

[18] B. Steder, R. B. Rusu, K. Konolige, and W. Burgard, "Point feature extraction on 3D range scans taking into account object boundaries," in *Proc. IEEE Int. Conf. Robot. Autom.*, May 2011, pp. 2061–2068.
[19] R. B. Rusu, N. Blodow, and M. Beetz, "Fast point feature histograms (FPFH) for 3D registration," in *Proc. IEEE Int. Conf. Robot. Autom.*, May 2009, pp. 3212–3217.
[20] A. Sehgal, D. Cernea, and M. Makaveeva, "Real-time scale invariant 3D range point cloud registration," in *Proc. Int. Conf. Image Anal. Recog.*, Jun. 2010, pp. 220–229.
[21] Z. Zhang, "A flexible new technique for camera calibration," *IEEE Trans. Pattern Anal. Mach. Intell.*, vol. 22, no. 11, pp. 1330–1334, Nov. 2000.
[22] J. Canny, "A computational approach to edge detection," *IEEE Trans. Pattern Anal. Mach. Intell.*, vol. PAMI-8, no. 6, pp. 679–698, Nov. 1986.
[23] C. Reich, R. Ritter, and J. Thesing, "3-D shape measurement of complex objects by combining photogrammetry and fringe projection," *Opt. Eng.*, vol. 39, pp. 224–231, Jan. 2000.
[24] X. Su, W. Chen, Q. Zhang, and Y. Chao, "Dynamic 3-D shape measurement method based on FTP," *Opt. Lasers Eng.*, vol. 36, pp. 49–64, Jul. 2001.
[25] S. Zhang, D. Van Der Weide, and J. Oliver, "Superfast phase-shifting method for 3-D shape measurement," *Opt. Express*, vol. 18, pp. 9684–9689, Apr. 2010.
[26] K. Liu, Y. Wang, D. L. Lau, Q. Hao, and L. G. Hassebrook, "Dual-frequency pattern scheme for high-speed 3-D shape measurement," *Opt. Express*, vol. 18, pp. 5229–5244, Mar. 2010.
[27] E. M. Stokely and S. Y. Wu,"Surface parametrization and curvature measurement of arbitrary 3-D objects: Five practical methods," *IEEE Trans. Pattern Anal.*, vol. 14, no. 8, pp. 833–840, Aug. 1992.
[28] M. Yang and E. Lee, "Segmentation of measured point data using a parametric quadric surface approximation," *Comput.-Aided Des.*, vol. 31, pp. 449–457, Jun. 1999.
[29] W. Ma and J. Kruth, "Parameterization of randomly measured points for least squares fitting of B-spline curves and surfaces," *Comput.-Aided Des.*, vol. 27, pp. 663–675, Sep. 1995.
[30] C. Cortes and V. Vapnik, "Support-vector networks," *Mach. Learn.*, vol. 20, pp. 273–297, Sep. 1995.
[31] J. A. Suykens and J. Vandewalle, "Least squares support vector machine classifiers," *Neural Process. Lett.*, vol. 9, pp. 293–300, Feb. 1999.
[32] O. Chapelle, P. Haffner, and V. N. Vapnik, "Support vector machines for histogram-based image classification," *IEEE Trans. Neural Netw.*, vol. 10, pp. 1055–1064, Sep. 1999.
[33] H. Drucker, D. Wu, and V. N. Vapnik, "Support vector machines for spam categorization," *IEEE Trans. Neural Netw.*, vol. 10, pp. 1048–1054, Sep. 1999.
[34] X. Chen, J. Xi, Y. Jin, and J. Sun, "Accurate calibration for a camera–projector measurement system based on structured light projection," *Opt. Lasers Eng.*, vol. 47, pp. 310–319, Mar./Apr. 2009.

Jing Xu (M'12) received the B.E. degree in mechanical engineering from Harbin Institute of Technology, Harbin, China, in 2003, and the Ph.D. degree in mechanical engineering from Tsinghua University, Beijing, China, in 2008.

He was a Postdoctoral Researcher in the Department of Electrical and Computer Engineering, Michigan State University, East Lansing, MI, USA. He is currently an Associate Professor in the Department of Mechanical Engineering, Tsinghua Unviersity. His research interests include vision-guided manufacturing, image processing, and intelligent robotics.

Rui Chen received the B.E. degree in mechanical engineering in 2014 from Tsinghua Unviersity, Beijing, China, where he is currently working toward the M.E. degree in the Department of Mechanical Engineering.

His research interests include three-dimensional measurement and cyber physical systems.

Heping Chen (M'00–SM'05) received the B.S. degree in control system engineering from Harbin Institute of Technology, Harbin, China, in 1989, the M.E. degree in electrical and electronic engineering from Nanyang Technological University, Singapore, in 1999, and the Ph.D. degree in electrical and computer engineering from Michigan State University, East Lansing, MI, USA, in 2003.

He was with the Robotics and Automation Laboratories, ABB Corporate Research, ABB, Inc., Windsor, CT, USA, from 2005 to 2010. He is currently an Assistant Professor in the Ingram School of Engineering, Texas State University, San Marcos, TX, USA. His research interests include micro/nanomanufacturing, micro/nanorobotics, industrial automation, and control system design and implementation.

Song Zhang received the B.S. degree from the University of Science and Technology of China, Hefei, China, in 2000, and the M.S. and Ph.D. degrees from Stony Brook University, Stony Brook, NY, USA, in 2003 and 2005, respectively, all in mechanical engineering.

He is currently an Associate Professor of mechanical engineering at Purde University, West Lafayette, IN, USA. His current research interests include developing superfast, super-resolution 3-D imaging technologies and exploring their applications, 3-D machine/computer vision, biophotonic imaging, virtual reality, augmented vision, human–computer interactions, forensic science, and biomedical engineering.

Ken Chen received the B.S. degree from Sichuan University, Chengdu, China, in 1982, and the M.S. and Ph.D. degrees from Zhejiang University, Hangzhou, China, in 1984 and 1987, respectively, all in mechanical engineering

From 1991 to 1992, he was a Visiting Professor with the University of Illinois, Chicago, IL, USA. From 1992 to 1995, he was a Postdoctoral Researcher with Purdue University, Indianapolis, IN, USA. He is currently a Professor in the Department of Mechanical Engineering, Tsinghua Unviersity, Beijing, China. His research interests include robotics and intelligent control, humanoid robots, microrobots and small robots, medical and space robots, manufacturing automation systems, and hydraulic servo systems.